# Duality-Based Transformer Model Including Eddy Current Effects in the Windings

Saeed Jazebi, *Member, IEEE*, and Francisco de León, *Fellow, IEEE*

*Abstract*—This paper presents a general method for building equivalent electric circuits of power transformers, including eddy current effects in windings and core. A high-frequency equivalent dual model for single- and three-phase transformers with two multilayer windings is derived from the application of the principle of duality. The model is built from elements available in circuit simulation programs, such as Electromagnetic Transients Program (EMTP)–Alternative Transients Program, EMTP-RV, PSCAD, and PSpice. The parameters of the frequency-dependent leakage inductance and winding resistance are computed with analytical formulae obtained from the solution of Maxwell's equations that are based on the geometrical dimensions and material information. Ideal transformers are utilized to isolate the electric components (winding resistors and capacitors) from the magnetic components (inductors). The physically correct connection points for electric and magnetic components are clearly identified. The proposed methodology is successfully validated versus finite-element simulations and laboratory measurements.

*Index Terms*—Eddy currents, electromagnetic transients, leakage inductance, principle of duality, transformer modeling.

## I. INTRODUCTION

TRANSFORMERS for power system applications are designed for the operating frequency (50/60 Hz). Nevertheless, during their life span, transformers may face very-high-frequency (VHF) transients up to 10 MHz. Therefore, models are required to predict their behavior at high frequencies to properly compute overvoltages, optimize the internal and external insulation design, and for insulation coordination.

Manufacturers of power-electronics devices are also interested in transformer models that accurately predict cross-regulation, transient performance, and high-frequency losses before prototyping. Finite-element methods are usually avoided due to the cost of the software, modeling complexity, and prolonged running time.

There are three general physical (topological) methods for system modeling: gyrator-capacitor models [1]–[5], bond graph models [6]–[9], and duality derived models [10]–[24]. In addition, there are some purely analytical [25]–[28] and circuit sim-

ulator methods [29]–[34] for the representation of eddy current effects in transformers.

In 1969, the capacitance-permeance analogy was introduced by Buntenbach [1]. Later, Hamill developed the technique to model magnetic components [2]. This approach was further extended to include nonlinearities in [3] and [4], and frequency-dependency behavior in [5]. One of the disadvantages of the gyrator-capacitor models is the absence of gyrators in Electromagnetic Transients Program (EMTP)-type programs.

Bond graph techniques [6], [7] are a graphical representation of energy flow in physical dynamic systems. Bond graphs are capable of representing electrical, magnetic, mechanical, thermal, and hydraulic systems. They are also capable of considering coupling effects between these different physical domains [8]. This method was utilized to model nonlinearities in electromagnetic devices in [8] and recently expanded to model transformers [9]. These models still require further development for compatibility with high-frequency simulations by representing eddy current and capacitive effects.

The principle of duality between magnetic and electric circuits was first introduced by Cherry [10] and further developed by Slemon [11]. There are many transformer models based on the principle of duality [12]–[24]. The leakage inductance of a single-phase three-winding transformer has been modeled with the direct application of the principle of duality in [20]. Later, the model has been extended for multiwinding transformers in [21]. The low-frequency behavior of these models has been enhanced for 2-, 3- and $n$-winding transformers in [22] and [23]. In this paper, the reversible model of [22] is further developed for midfrequency studies considering the effects of eddy currents in the windings and iron core together with capacitive couplings.

The main contribution of this paper is to include eddy current effects in the dual reversible model of [20] to produce a midfrequency model. A general method to derive the equivalent circuit of any type of transformer is presented. Analytical formulae are derived for the calculation of the model parameters for multilayer cylindrical windings. The frequency-dependent parameters of the leakage inductance and winding resistances can be calculated from the transformer geometry and material information. Physically correct connection points are determined for the interturn and interlayer capacitors. The model is based on simple circuit elements and can be easily assembled in circuit simulator programs, such as EMTP and PSpice, using only readily available circuit elements.

Since the model is completely dual, each node represents a physical point in the transformer that makes it ideal for transformer designers. The model presented in this paper is useful
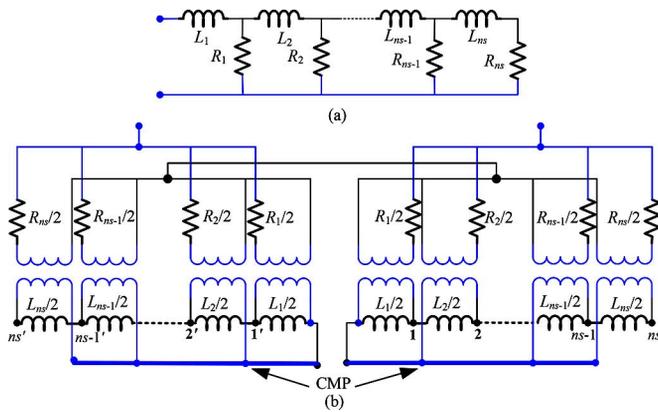
Fig. 1. Physical Cauer circuits for a discretized single-layer winding: (a) single-sided model and (b) double-sided model. Note that all circuit elements of the double-sided model have half the value of the single-sided model. CMP = common magnetic point.



Fig. 2. Top view of a rectangular two-layer spiral coil showing the electrical connections of the ideal transformers. Trimmed with dashed lines is a 2-section example of the model presented in Fig. 1(b).

for power-electronics designers, transformer manufacturers, as well as power system designers and analysts.

## II. SINGLE-SIDED VERSUS DOUBLE-SIDED PHYSICAL CAUER CIRCUITS

A physical dual model for the representation of the eddy current effects in transformer windings is shown in Fig. 1(a) [24]. This model is only capable of representing a single layer of a winding and is derived from the direct application of the principle of duality on only one side of the winding. From comprehensive studies on modeling eddy currents in transformer windings, we have observed that it is necessary to have access to the terminals of each subdivision of the model in order to add capacitive effects between layers and between windings.

Fig. 1(b) shows an equivalent circuit of the model of Fig. 1(a) that gives access to the connection points. The model isolates the magnetic components (inductors) form the electric components (resistors). Note that the capacitors can be connected to the terminals and are consequently isolated from the magnetic circuit. The inductors obtained from the principle of duality represent the magnetic behavior of the windings rather than the electrical behavior. These components model the distribution of the magnetic flux. However, resistors and capacitors deal with the flow of the electric charge. In other words, currents in inductors correspond to magnetic flux and currents in capacitors and resistors correspond to the flow of electric charges. The two phenomena are of a completely different nature.

The model presented in Fig. 1(b) is derived from the direct application of the principle of duality on two sides of the winding [20]. Fig. 2 presents a two-layer coil to describe how the topological dual model of Fig. 1(a) is obtained. A single layer of a winding should be discretized into several subsections to obtain the model of Fig. 1(b). In Fig. 2, each layer is sectionalized into only two sections instead of the $n$-sections because of a lack of space. Each subdivision is represented by a linear inductor, an ideal transformer, and a resistor.

The model is symmetric with respect to the vertical axis as shown in Fig. 2. The double-sided model divides a single turn of a wire into two (series-connected) identical conductors. As shown, the two ideal transformers representing half a layer need
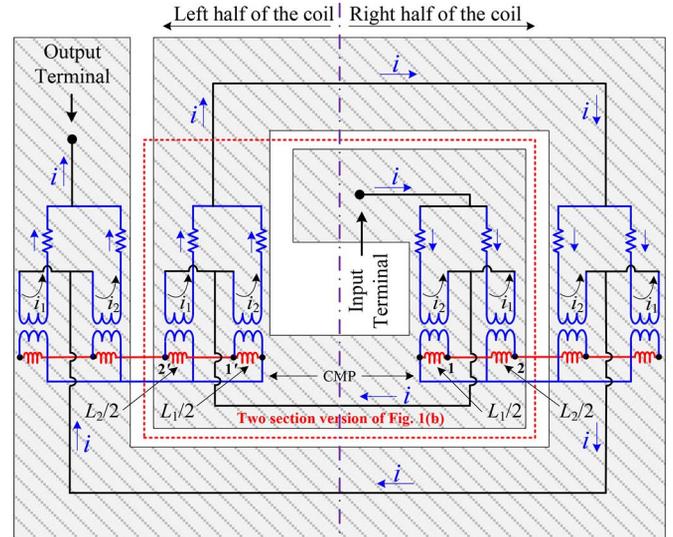
to be connected in parallel, since the current flows naturally in the two parallel subsections. This is because a single conductor is discretized into two sections in this figure. The set of ideal transformers on the right- and left-hand sides of the model (for the same layer) needs to be connected in series since they represent series sections of a single turn. Therefore, the model parameters of Fig. 1(b) are half the values of parameters of Fig. 1(a). (See [24].) This is so because half of the magnetic and electric energy flows on each side of the model.

As can be observed, the advantage of the double-sided Cauer is the accessibility to all required terminals. Inductors are fed through ideal transformers from the source. Note that the first terminal of the ideal transformers is connected to the inductors and the second terminal is connected to the common magnetic point (CMP). For example, the first (inner) ideal transformer only excites the first inductor. However, the second ideal transformer excites the first and the second inductors concurrently. This pattern is applied to all other ideal transformers and inductors to properly represent the proximity effects. This is in accordance with Amperes' law, where the enclosed current is what produces the magnetic field. Thus, the current flowing in the last section creates a magnetic field in all sections. However, the currents in inner sections only create a magnetic field in the excited section and all internal sections.

To validate the equivalence of the two circuits (single-sided and double-sided) for different model orders over a wide frequency range, numerous EMTP simulations were carried out. Fig. 3 shows a sample of these studies for a single layer of the outer winding with 6-mm thickness. These simulation results show the perfect equivalence of the two models to represent resistance and inductance of a single layer. The graphs are only presented for frequencies up to 10 kHz. Beyond this frequency, the capacitive effects change the electromagnetic behavior of the coils and, thus, they need to be considered. However, the model of this paper is completely general and accurately represents the behavior of inductance and resistance for higher frequencies using higher order models as shown in Section IV.
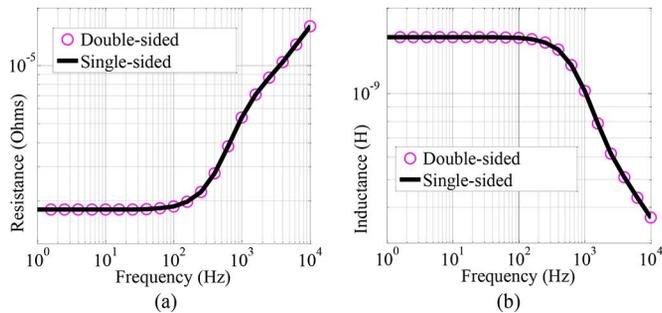
Fig. 3. Comparison of the single- and double-sided Cauer models for a conductor with $d = 6$ mm, $l_w = 1$ m, $r_{\text{in}} = 0.1$ m with $n_s = 5$ subsections: (a) resistance and (b) inductance.

## III. EQUIVALENT CAUER CIRCUIT FOR MULTILAYER WINDINGS AND CALCULATION OF MODEL PARAMETERS

In this section, a dual model for multilayer windings is derived as an extension of the double-sided equivalent circuit of Fig. 1. The model for a single-phase two-winding transformer is presented in Fig. 4. For illustration, it is assumed that each winding has only two layers, and each layer is modeled with only two subsections. The dual electric circuit is drawn on top of the winding from the direct application of the principle of duality. Note that the region between layers/windings (insulation or cooling ducts) is represented with linear inductors. Also, interlayer and interwinding capacitive effects could be added to the terminals as illustrated in Fig. 4.

### A. Determination of Winding Model Parameters

In the frequencies near dc $(\omega \rightarrow 0)$, the magnetic field is uniformly distributed in the transformer windings. Due to eddy current effects, the magnetic field becomes nonuniform for higher frequencies. However, the field can be considered uniform in a sufficiently thin conductor slice cut along the conductor thickness [17]. This is correct when the penetration depth $(\delta = \sqrt{2/\omega\mu\sigma})$ is (much) larger than the thickness of the subdivision. Theoretically, if the conductor is discretized into an infinite number of thin subsections, the variation of the magnetic field in each section could be neglected and considered constant (dc). Thus, a frequency dependent inductance could be represented with several constant low-frequency (dc) inductances of a topologically correct synthesized circuit [17], [24], [37], [38]. Therefore, for the calculation of parameters, each layer is discretized into $n_s$ thin subsections as shown in Fig. 5. The equivalent electric circuit for windings (leakage inductance and coil resistance) is developed from the solution of the electromagnetic-field problem in dc $(\omega \rightarrow 0)$. Note that in Fig. 5 the windings have $n_l$ layers, but only two layers are shown. In this figure, $s$ and $k$ stand for subsections and layers, respectively.

The model parameters are computed from the solution of the electromagnetic-field problem inside the conductors in cylindrical coordinates as in [24]. The magnetic field is assumed to be completely axial. One can write the diffusion equation in cylindrical coordinates for dc as follows [35]:

$$r^2 \frac{\partial^2 H_z(r,t)}{\partial r^2} + r \frac{\partial H_z(r,t)}{\partial r} = 0. \tag{1}$$
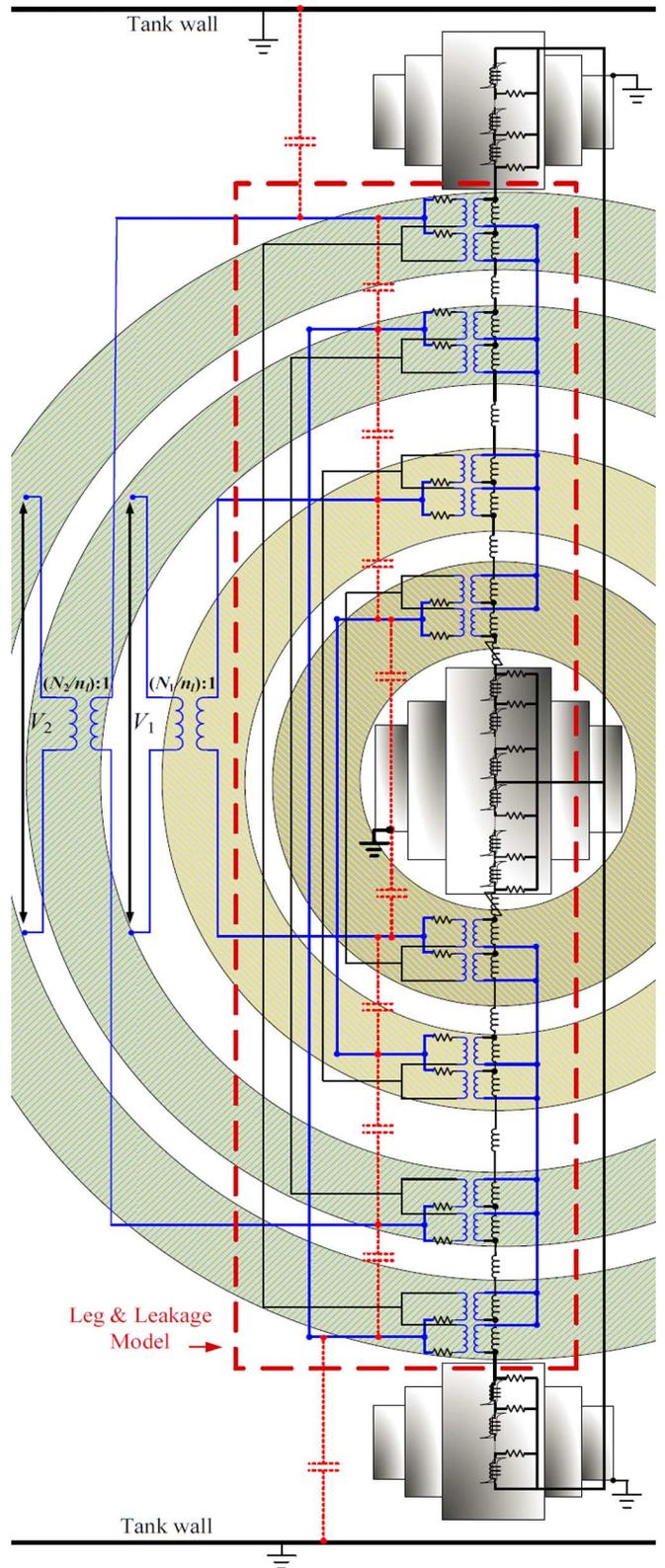


Fig. 4. Derivation of the equivalent electrical circuit for a single-phase two-winding shell-type transformer (cut view of the winding and core structure). The leg and leakage model are used in Section V to assemble the three-phase models.

Equation (1) is an Euler partial differential equation. Parameters $H_z, r, t$ are the magnetic-field strength in the $z$ direction,

radial distance from the center, and time, respectively. Per Ampere's law, the boundary conditions for the outer winding are

$$H_z(r_{k-1},t) = \frac{(k-1)I}{l_w} \quad \text{and} \quad H_z(r_k,t) = \frac{kI}{l_w} \quad (2)$$

where $l_w$ is the height of the winding. The solution of (1) for the outer winding is

$$H_z(r) = \frac{kI}{l_w} + \frac{I\ln(r/r_k)}{l_w \ln(r_k/r_{k-1})}. \quad (3)$$

The current in each subsection is derived from the expression of the current density

$$J = \nabla \times H = \frac{I}{l_w \ln(r_k/r_{k-1})r}\,\widehat{\varphi} \quad (4)$$

$$I_{s,k} = \int_0^{l_w} \int_{r_s}^{r_{s-1}} J\,dz\,dr = \frac{\ln(r_{s-1}/r_s)}{\ln(r_k/r_{k-1})}I := M_{s,k}I. \quad (5)$$

$M_{s,k}$ is a factor that considers the cylindrical geometry of the windings. Consequently, the corresponding inductance of each subsection for the outer winding is obtained from the magnetic energy as follows:

$$L_{\text{dc},s,k} = \frac{2W_{s,k}}{I_{s,k}^2} = \int_0^{2\pi}\int_0^{l_w}\int_{r_s}^{r_{s-1}} \frac{\mu H^2(r)r\,d\varphi\,dr\,dz}{I_{s,k}^2}$$

$$= \frac{\mu\pi}{l_w \ln^2\left(\frac{r_{s-1}}{r_s}\right)}$$

$$\times \left\{ \begin{array}{l} r_{s-1}^2 \left[ \begin{array}{l} \left(k\ln\left(\frac{r_{k-1}}{r_k}\right) + \ln\left(\frac{r_k}{r_{s-1}}\right)\right)^2 \\ +k\ln\left(\frac{r_{k-1}}{r_k}\right) + \ln\left(\frac{r_k}{r_{s-1}}\right) + 0.5 \end{array} \right] \\ -r_s^2 \left[ \begin{array}{l} \left(k\ln\left(\frac{r_{k-1}}{r_k}\right) + \ln\left(\frac{r_k}{r_s}\right)\right)^2 \\ +k\ln\left(\frac{r_{k-1}}{r_k}\right) + \ln\left(\frac{r_k}{r_s}\right) + 0.5 \end{array} \right] \end{array} \right\}$$

$$(6)$$

where $\mu$ is the magnetic permeability. The consistency of (6) could be checked with the following equation according to [24, App. A] considering the effect of curvature:

$$L_{\text{DC},k} = \sum_{s=1}^{n_s} M_{s,k}^2 L_{\text{dc},s,k} \quad (7)$$

where $L_{\text{DC},k}$ is the dc inductance of the $k$th layer [24]. Suppose that the dc inductance of a complete multilayer winding is $L_{\text{DC}}$, then, this inductance could be computed from the total magnetic energy $(W)$ in the winding volume. The total current that produces the magnetic energy in the $n_l$ layers is $n_lI$, therefore

$$L_{\text{DC}} = \frac{2W}{(n_lI)^2} = \frac{1}{n_l^2}\frac{2(W_1 + \cdots W_k + \cdots W_{n_l})}{I^2} \quad (8)$$

where $W_k$ is the magnetic energy of the $k$th layer and $n_l$ is the number of winding layers. Equation (8) could be expanded with the energy of the different subsections as

$$L_{\text{DC}} = \frac{1}{n_l^2}\left( \frac{2w_{1,1}}{I^2} + \frac{2w_{2,1}}{I^2} + \cdots \frac{2w_{n_s,1}}{I^2} \right.$$

$$\left. + \cdots \frac{2w_{s,k}}{I^2} + \cdots \frac{2w_{n_s,n_l}}{I^2} \right) \quad (9)$$

where $w_{s,k}$ is the magnetic energy of the $s$th subsection of the $k$th layer. Substituting (5) in (9), and considering $L_{\text{dc},s,k} = 2W_{s,k}/I_{s,k}^2$ according to (6), the following expression is obtained:

$$L_{\text{DC}} = \frac{1}{n_l^2}\left( \begin{array}{l} M_{1,1}^2 L_{\text{dc},1,1} + M_{2,1}^2 L_{\text{dc},2,1} + \cdots M_{n_s,1}^2 L_{\text{dc},n_s,1} \\ + \cdots M_{s,k}^2 L_{\text{dc},s,k} \cdots M_{n_s,n_l}^2 L_{\text{dc},n_s,n_l} \end{array} \right)$$

$$= L'_{\text{dc},1,1} + L'_{\text{dc},2,1} + \cdots L'_{\text{dc},n_s,1} + \cdots$$

$$L'_{\text{dc},s,k} \cdots L'_{\text{dc},s,k} \cdots L'_{\text{dc},n_s,n_l}. \quad (10)$$

Thus, from (10), to compute $L_{\text{DC}}$ from $L_{\text{dc},s,k}$, the inductances should be refined to $L'_{\text{dc},s,k}$ with the following expression:

$$L'_{\text{dc},s,k} = \frac{1}{n_l^2}M_{s,k}^2 L_{\text{dc},s,k}. \quad (11)$$

To compute the correct $L_{\text{DC}}$ from the terminals of the Cauer model, inductances computed with (11) need a refinement to consider the proximity effect. A complete description for the proximity effect coefficients is available in [24, App.]. These coefficients are functions of sums and products of resistances of winding subsections. The following expression is obtained after combining the proximity effect coefficients and (11) for the inductances of the Cauer circuit:

$$L_{s,k} = \frac{M_{s,k}^2}{2n_l^2}\left\{ \frac{\sum_{p=1}^{n_t}\left(\prod_{\substack{j=1 \\ j\neq p}}^{n_t}(R_j)\right)}{\sum_{p=s}^{n_t}\left(\prod_{\substack{j=1 \\ j\neq p}}^{n_t}(R_j)\right)} \right\}^2 L_{\text{dc},s,k} \quad (12)$$

where $n_t = n_l \times n_s$ is the total number of subsections of the winding, and coefficient 2 in the dominator modifies the values for the two-sided Cauer model (see Fig. 1). Resistors $R_j(j = 1, 2, \ldots n_s, n_s + 1, \ldots n_s \times n_l)$ could be substituted by the corresponding values

$$R_j = R_{s,k} = \frac{1}{2}\frac{l_{s,k}}{\sigma A_{s,k}} = \frac{\pi r_{\text{mean},s,k}}{\sigma l_w d_{s,k}} = \frac{\pi(r_{s-1,k} + r_{s,k})}{2\sigma l_w(r_{s-1,k} - r_{s,k})} \quad (13)$$

where $\sigma$ is the material electrical conductivity and $d_{s,k}$ is the thickness of the subsection. Finally, the inductance in layer $k$ and subsection $s$ can be calculated from

$$L_{s,k} = \frac{M_{s,k}^2}{2n_l^2}\left\{ \frac{\sum_{p=1}^{n_t}\left(d_p\prod_{\substack{j=1 \\ j\neq p}}^{n_t}(r_{\text{mean},j})\right)}{\sum_{p=s}^{n_t}\left(d_p\prod_{\substack{j=1 \\ j\neq p}}^{n_t}(r_{\text{mean},j})\right)} \right\}^2 L_{\text{dc},s,k} \quad (14)$$

where $d_p = d_{s,k}$, $p = s \times k$, $s = 1, 2, \ldots n_s$, $k = 1, 2, \ldots n_l$; thus, $p = 1, 2, \ldots n_s, n_s + 1, \ldots n_s \times n_l$. Therefore, all parameters (resistors and inductors) of the outer winding of Fig. 4 can be calculated with (13) and (14), respectively, using (5) and
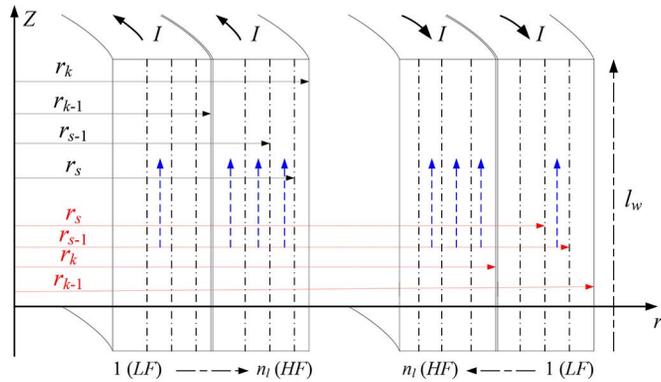
Fig. 5. Transformer windings with $k$ layers and $s$ subsections. Note that the indices for inner and outer windings are exchanged to use the same model equations for both windings.



Fig. 6. (a) Magnetic-field strength for a two-layer winding (outer coil), thickness of each conductor $d = 4$ mm and (b) discretization of the conductor according to the distribution of the magnetic field for high frequencies. Note that for an $n$-layer winding, the field pattern for the 3rd to $n$th layer is the same as that for the second layer. Only the first layer shows different magnetic behavior.

(6). These equations are only functions of coil parameters (dimensions and number of turns). Note that to use the same set of formulae for the inner winding, it is necessary to exchange the indices of the layers and subsections according to Fig. 5.

Accordingly, all inductances of Fig. 4 are computed for $N = 1$. Also, as discussed before, the turns ratio of the ideal transformers connected to the inductors is 1:1. The model of Fig. 4 represents $n_l$ turns of solid conductors. These conductors consist of $N_1/n_l$ and $N_2/n_l$ turns in the primary and secondary, respectively. Therefore, two ideal transformers with ratios $N_1/n_l : 1$ and $N_2/n_l : 1$ are added to the terminals (see Fig. 4).

### B. Layer Discretization Pattern

Ladder-type models require an infinite number of sections to exactly represent the physical behavior of the eddy currents in the windings. Acceptable engineering accuracy could be reached with a finite number of sections over a finite frequency range. To synthesize an optimum circuit, three rules need to be followed: 1) to obtain higher accuracy, higher order models are needed; 2) for a higher frequency model, higher order circuits need to be retained; 3) higher order models lead to a higher computation effort in circuit simulation programs. Therefore, the lowest circuit order that does the job should be selected. Also, for high-frequency transients (small penetration depths), it is recommended to use thinner layers at the turn edges. This is so because in these regions, the current density, the magnetic field, and the magnetic energy are higher and vary the most. However, only a small amount of field would reach the inner layers of the turn. Therefore, the thickness of the layer can be increased from the edges to the inner layers to reduce the model order without affecting accuracy.

In [24], the authors have proposed optimizing the circuit order and the discretization pattern for different types of transients, for example, low-, mid-, and high-frequency studies with acceptable engineering accuracy. This is so because for different frequency ranges, models with different orders and different discretization pattern give acceptable performance and computation time with small error. Note that lower order models perform accurately only for low-frequency transients, while higher

order models always work for low frequencies at the cost of higher computational burden.

The magnetic-field behavior is different in a multilayer winding compared to a single-layer winding. Fig. 6(a) shows the amplitude of the magnetic field along the thickness of the two-layer winding (outer) for different frequencies. As discussed in the previous section, the layers are numbered from the outermost to the innermost for the outer winding. The first layer always has its maximum field in the proximity of the second layer and eventually the field decays to zero. Therefore, the first layer can be discretized according to the guidelines presented in [24]. Layers 2 to $k$ have different behavior due to the proximity effect. At low frequencies, the magnetic field decays linearly. However, one can see that the graph bends for higher frequencies and has its minimum toward the center of the layer. Therefore, it is recommended to discretize these $k - 1$ layers with thicker layers in the middle of the conductor and thinner layers at the edges. For example, a two-layer winding (each 4 mm) is discretized for slow front transients in Fig. 6. The thicknesses are extracted from [24, Table II]. The outer layer (first) is discretized for $d = 4$ mm. The inner layer (second) is divided into two equal sections. Each section is discretized according to the information in [24] for $d = 2$ mm.

### C. Insulation

The inductances of the space between layers (insulation) or between the two windings can be approximated with [20]

$$L_{\text{ins}} = \frac{2\pi\mu_0\, r_{\text{mean,ins}}\, d_{\text{ins}}}{l_w} \tag{15}$$

where $r_{\text{mean,ins}}$ is the mean radius of the insulation layer, $l_w$ is the height of the windings, and $d_{\text{ins}}$ is the thickness of the insulation. This inductance needs to be divided by 2 to be assigned
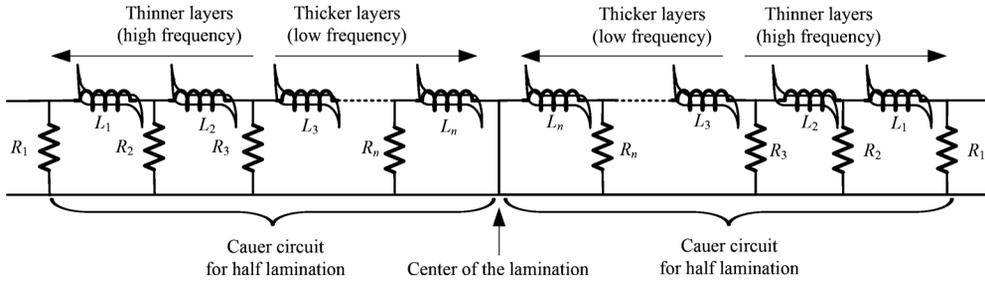
Fig. 7. Topology of a duality-derived back-to-back Cauer model for the representation of the center leg.

to the two sides of the model. Assuming long cylindrical windings, the capacitances between layers or between windings can be computed from [40]

$$C_{\text{ins}} = \left(2\pi\varepsilon\, l_w N^2\right) / \left(n_l^2 \ln(r_2/r_1)\right) \qquad (16)$$

where $r_1$ is the outer radius of the inner layer, $r_2$ is the inner radius of the outer layer, $N$ is the number of turns, and $\varepsilon$ is the permittivity of the insulation. Note that, according to Fig. 4, half of this value is assigned for each capacitance on the two sides of the model. The coefficient $(N/nl)^2$ is multiplied because the capacitors are placed behind the ideal transformer with $N/nl$ turns ratio (see Fig. 4).

### D. Iron Core

The physically correct representation of the iron core for high frequencies is the conventional Cauer circuit that is derived from the principle of duality. The terminal impedance of this model tends to zero for low frequencies and, therefore, correctly represents the lack of losses in the core at dc [24]. This circuit is well-known and has been implemented in [16] and [36]–[39]. Note that the circuit elements of the Cauer model near its terminals dominantly affect the high-frequency behavior of the core. The elements that are far from the terminals represent the low-frequency response. Fig. 4 shows the physically correct connections of the conventional Cauer circuits to the transformer model. The yokes and external limbs are modeled with single conventional Cauer circuits.

The low-frequency region of the center leg is geometrically located at the middle point. Therefore, two back-to-back Cauer circuits properly represent the center leg. According to this, the center leg could be discretized finer at the edges and coarser in the center. This technique allows discretizing the core symmetrically, which reduces the order of the final equivalent circuit and, thus, the computation time (since the alternative is to use a fine discretization for the entire lamination). At high frequencies, the concentration of the magnetic flux is higher at the edges of the center leg where the behavior could be correctly seen with the relative increase of current distribution in the last sections of the Cauer circuit (for example, $R_1$ and $L_1$). Fig. 7 describes how a back-to-back Cauer circuit is constructed.

## IV. MODEL VALIDATION

In this section, the frequency response of the dual model of Fig. 4 is evaluated versus finite-element simulations and laboratory measurements.
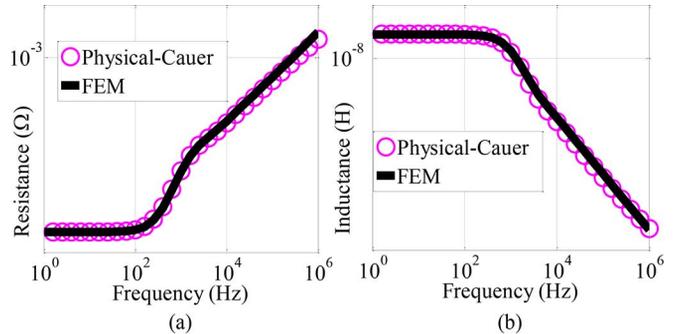


Fig. 8. Frequency response of the transformer model in short-circuit conditions for $d = 4$ mm, $n_l = 2$, $n_s = 12$, $l_w = 1$ m, $d_{\text{ins}} = 5$ mm, $r_{\text{in\_inner\_winding}} = 87$ mm, $r_{\text{in\_outer\_winding}} = 100$ mm: (a) resistance and (b) inductance.
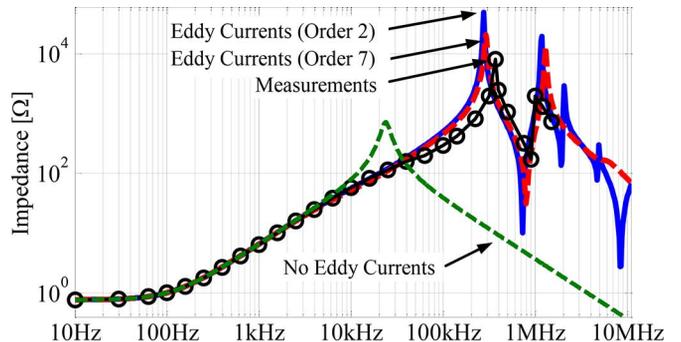


Fig. 9. Comparison of the measurement and simulation of impedance magnitude for a single-phase transformer in short-circuit conditions.

### A. Validation versus FEM

A short-circuit test is simulated with FEM for a two-winding transformer with the same number of turns in the primary and secondary. The inner winding is shorted and the outer winding is excited. The thickness of each of the two windings is $d = 4$ mm. Fig. 8 shows the comparison of the equivalent resistance and inductance obtained from EMTP and FEM simulations. The results demonstrate the high accuracy of the model for the target frequency range (from 1 Hz to 1 MHz).

### B. Validation versus Measurements

A laboratory single-phase 1 kVA transformer with the geometrical information presented in [22] is modeled. The model order is selected according to the optimized parameters for both slow front and fast front transients in [24]. Accordingly, because the thickness of each layer is 1.61 mm, the model order is
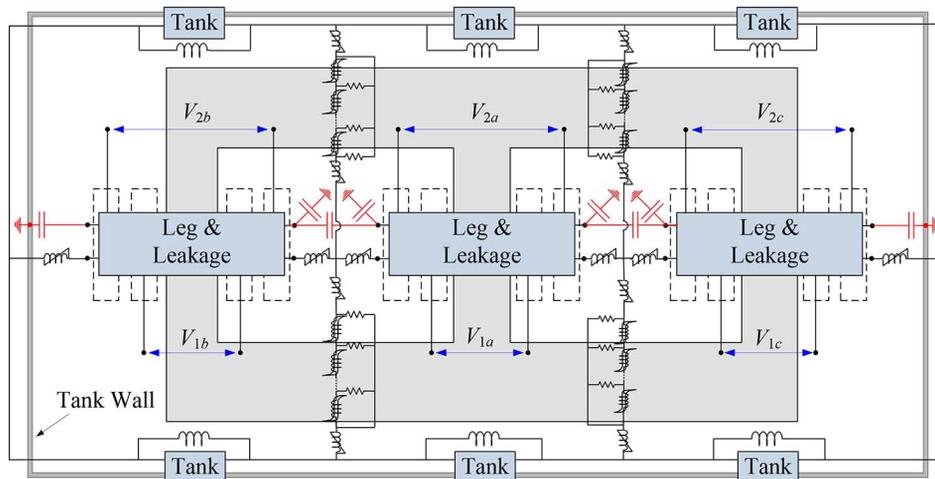
Fig. 10. Topological dual representation of a three-phase core-type transformer, including eddy current effects, capacitive effects, and tank. The leg and leakage model is taken from Fig. 4. Y-$\Delta$ connections shall be made after the addition of ideal transformers to the terminals.

$n_s = 2$ for slow front transients ($f \leq 10$ kHz) and $n_s = 7$ for fast front transients ($f \leq 1$ MHz). The insulation between different layers and between the windings is modeled with the inductors and capacitors computed with (15) and (16). A fill factor $K_u = 0.6$ is considered to account for the effect of round conductors and insulation between consecutive turns in different layers. In this way, the dc resistance and dc inductance between the model and simulation match. Fig. 9 shows the frequency response of the transformer in a short circuit between the innermost and outermost windings. Laboratory measurements are only available for frequencies up to 2 MHz. One can observe a good agreement between measurements and simulations. The largest differences of the resonant frequencies between measurements and simulations are about 20%. These differences are caused by the modeling approximations, uncertainties in the material properties (permittivity of the paper insulation), and transformer manufacturing tolerances. Since all parameters are derived from the geometry and material information of the transformer, the method is applicable to single-phase transformers of any size.

The results indicate that the model with two sections (optimized for 10 kHz) seems to be adequate to represent the transformer for higher frequencies up to 1 MHz. This is so because the effect of capacitors is strongly dominant in the impedance at higher frequencies. However, more research is necessary to draw general conclusions on this subject. At frequencies higher than 1 MHz, the need to use a higher order model becomes evident, and the difference between the high- and low-order models becomes significant. The low-order model (order 2) shows resonant frequencies at around 2, 5, and 9 MHz. However, the high-order model (order 7) shows a single resonance at around 15 MHz (not shown). Therefore, as expected, the low-order model is not capable of predicting the inductive behavior of the coils for very high frequencies.

As discussed earlier, the eddy currents (proximity and skin effects) are the main reason of the changes in the electromagnetic behavior of transformers in different frequencies. The frequency response of the model without eddy current effects is also presented in Fig. 9. This comparison shows the significance of the eddy currents for high-frequency models.

## V. THREE-PHASE TRANSFORMERS

The transformer tank significantly affects the transformer behavior in three operating conditions:
- overexcitation of the windings;
- zero-sequence conditions and unbalances;
- overexcitation and zero sequence simultaneously, for example, in the case of half-cycle saturation due to GIC.

The dual model presented in Section III (Fig. 4) can be extended to three-phase transformers. The topology of the "leakage and leg model" (trimmed with dashed lines in Fig. 4) is identical for all three phases. Figs. 10 and 11 show the construction of the dual frequency-dependent model developed for the three- and five-leg transformers. The proper connection of the frequency-dependent tank model is also depicted in Figs. 10 and 11. The tank could be represented with the models of [46]–[48]. In low frequencies ($\omega \to 0$), there are not eddy currents induced in the transformer tank. Therefore, it is recommended to use conventional Cauer (as for the iron core) instead of physical Cauer circuits for the representation of the frequency-dependent behavior of the tank. For three-phase transformers, further considerations and special methods are needed to take into account the zero-sequence impedance. Also, for a reversible model, the high saturation parameters of such models need to be modified. The methods for the determination of the parameters and the validation results will be presented in an upcoming paper for the three-phase models of Figs. 10 and 11.

## VI. DISCUSSION

Simulation and measurement results indicate that the model is accurate for a wide range of frequencies (dc to MHz), therefore it is applicable to power system transient studies and the design of transformers for power systems or power-electronics devices.

For power-electronics applications, it is usually assumed that the core and windings work at frequency ranges where the penetration depth is larger than the thickness of the construction elements. Hence, to avoid losses due to eddy current effects in the operating frequencies, ferrite cores and Litz wires are
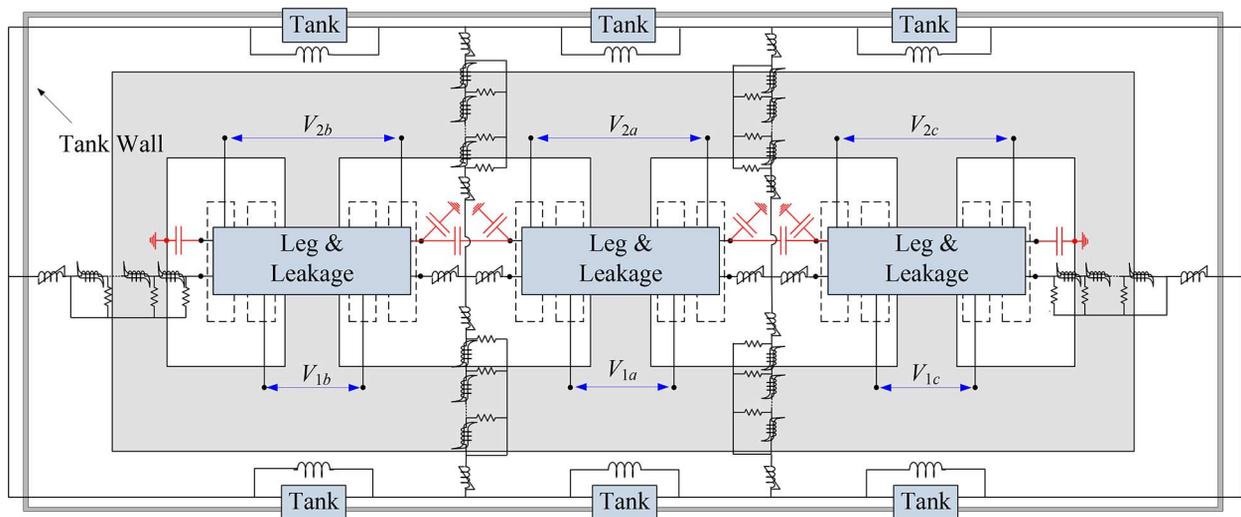
Fig. 11. Topological dual representation of a three-phase five-leg transformer, including eddy current effects, capacitive effects, and tank. The leg and leakage model is taken from Fig. 4. Y-Δ connections shall be made after the addition of ideal transformers to the terminals.

commonly used. However, the design of the compact high-frequency switching supplies is also driven by several other factors, such as size, efficiency, and reliability [40]. Frequently, the windings of these transformers carry currents with large dc components. Litz wires are suitable for high-frequency currents but they are not ideal for dc current. The total copper loss in dc could be reduced by packing more copper in the available space (use of solid wires). Therefore, the high-frequency model, including eddy current effects, introduced in this paper is a helpful tool for the design of transformers for power-electronics applications [41]–[45].

The model proposed in this paper allows for the calculation of the electromagnetic field at different locations of the transformer. This is so because the voltage drops across the model inductors are analogous to the magnetic fluxes circulating in the corresponding construction element of the transformer; see [24]. The currents flowing in each winding section correspond to currents in the model resistors. Therefore, the circuit can give a precise and accurate understanding of the electromagnetic behavior of the transformer components at high frequencies. This makes the model an easy-to-use tool to design high-frequency magnetic components of power-electronics devices.

A similar detailed model could be synthesized to represent the transformer capacitive effects to take into account the distribution of the voltage across the insulation of the windings for mid- and high-frequency transients, for example, switching or impulse transient voltages. These models are helpful for the design of the transformer insulation system.

The determination of the core parameters and tank models, including hysteresis effects, eddy currents, and excess losses will be presented in an upcoming paper.

## VII. CONCLUSION

A physically consistent transformer model that includes the effects of eddy currents has been derived based on the principle of duality. Only elements available in circuit simulators

are necessary to build a model that is valid over a wide frequency range. Analytical formulae have been presented to calculate the parameters of the winding model from the geometrical construction and material information. The accuracy of the model has been verified by comparison with finite-element simulations and laboratory measurements. The correct connection of the frequency-dependent iron-core elements and capacitive couplings has been revealed. The model is capable of accurately representing the leakage inductance, copper losses, as well as skin and proximity effects.

The final objective of this continuous research is to obtain a general modeling approach for transformers from the application of the principle of the duality. It is believed that the model presented in this paper can be further extended to multiwinding transformers with any core geometry or winding configuration and connection.

## REFERENCES

[1] R. W. Buntenbach, "Analogs between magnetic and electrical circuits," *Electron Prod.*, vol. 12, no. 5, pp. 108–113, Oct. 1969.

[2] D. C. Hamill, "Lumped equivalent circuits of magnetic components: The gyrator-capacitor approach," *IEEE Trans. Power Electron.*, vol. 8, no. 2, pp. 97–103, Apr. 1993.

[3] D. C. Hamill, "Gyrator-capacitor modeling: A better way of understanding magnetic components," in *Proc. IEEE Appl. Power Electron. Conf. Expo.*, 1994, pp. 326–332.

[4] P. G. Blanken and J. J. L. M. van Vlerken, "Modeling of electromagnetic systems," *IEEE Trans. Magn.*, vol. 27, no. 6, pp. 4509–4515, Nov. 1991.

[5] P. G. Blanken, "A lumped winding model for use in transformer models for circuit simulation," *IEEE Trans. Power Electron.*, vol. 16, no. 3, pp. 445–460, May 2001.

[6] D. C. Kamopp, D. L. Margolis, and R. C. Rosenberg, *System Dynamics: A Unified Approach*, 2nd ed. Hoboken, NJ, USA: Wiley, 1990.

[7] P. C. Breedveld, R. C. Rosenberg, and T. Zhou, "Bibliography of bond graph theory and applications," *J. Franklin Inst.*, vol. 328, no. 5/6, pp. 1067–1087, 1991.

[8] H. Fraisse, J. P. Masson, F. Marthouret, and H. Morel, "Modeling of a non-linear conductive magnetic circuit Part 2: Bond graph formulation," *IEEE Trans. Power Electron.*, vol. 31, no. 6, pp. 4068–4070, Nov. 1995.

[9] G. Gonzalez-A and D. Nuñez-P, "Electrical and magnetic modeling of a power transformer: A bond graph approach," *World Acad. Sci., Eng. Technol.*, vol. 6, no. 9, pp. 591–597, 2012.

[10] E. C. Cherry, "The duality between interlinked electric and magnetic circuits and the formation of transformer equivalent circuits," *Proc. Phys. Soc.*, vol. (B) 62, pp. 101–111, Feb. 1949.

[11] G. R. Slemon, "Equivalent circuits for transformers and machines including nonlinear effects," *Proc. Inst. Elect. Eng.*, vol. 100, no. 5, pp. 129–143, 1953, IV.

[12] J. A. Martínez, R. Walling, B. Mork, J. Martin-Arnedo, and D. Durbak, "Parameter determination for modeling systems transients. Part III: Transformers," *IEEE Trans. Power Del.*, vol. 20, no. 3, pp. 2051–2062, Jul. 2005.

[13] J. A. Martínez and B. Mork, "Transformer modeling for low and mid-frequency transients—A review," *IEEE Trans. Power Del.*, vol. 20, no. 2, pt. 2, pp. 1625–1632, Apr. 2005.

[14] F. de León and A. Semlyen, "Complete transformer model for electromagnetic transients," *IEEE Trans. Power Del.*, vol. 9, no. 1, pp. 231–239, Jan. 1994.

[15] A. Narang and R. H. Brierley, "Topology based magnetic model for steady-state and transient studies for three phase core type transformers," *IEEE Trans. Power Syst.*, vol. 9, no. 3, pp. 1337–1349, Aug. 1994.

[16] F. de León and A. Semlyen, "Time domain modeling of eddy current effects for transformer transients," *IEEE Trans. Power Del.*, vol. 8, no. 1, pp. 271–280, Jan. 1993.

[17] P. Holmberg, M. Leijon, and T. Wass, "A wideband lumped circuit model of eddy current losses in a coil with a coaxial insulation system and a stranded conductor," *IEEE Trans. Power Del.*, vol. 18, no. 1, pp. 50–60, Jan. 2003.

[18] B. A. Mork, F. Gonzalez, D. Ishchenko, D. L. Stuehm, and J. Mitra, "Hybrid transformer model for transient simulation—Part I: Development and parameters," *IEEE Trans. Power Del.*, vol. 22, no. 1, pp. 248–255, Jan. 2007.

[19] B. A. Mork, F. Gonzalez, D. Ishchenko, D. L. Stuehm, and J. Mitra, "Hybrid transformer model for transient simulation—Part II: Laboratory measurements and benchmarking," *IEEE Trans. Power Del.*, vol. 22, no. 1, pp. 256–262, Jan. 2007.

[20] F. de León and J. A. Martinez, "Dual three-winding transformer equivalent circuit matching leakage measurements," *IEEE Trans. Power Del.*, vol. 24, no. 1, pp. 160–168, Jan. 2009.

[21] C. Álvarez-Mariño, F. de León, and X. M. López-Fernández, "Equivalent circuit for the leakage inductance of multi-winding transformers: Unification of terminal and duality models," *IEEE Trans. Power Del.*, vol. 27, no. 1, pp. 353–361, Jan. 2012.

[22] S. Jazebi, F. de León, A. Farazmand, and D. Deswal, "Dual reversible transformer model for the calculation of low-frequency transients," *IEEE Trans. Power Del.*, vol. 28, no. 4, pp. 2509–2517, Oct. 2013.

[23] S. Jazebi and F. de León, "Experimentally validated reversible single-phase multi-winding transformer model for the accurate calculation of low-frequency transients," *IEEE Trans. Power Del.*, vol. 30, no. 1, pp. 193–201, Feb. 2015.

[24] S. Jazebi, F. de León, and B. Vahidi, "Duality-synthesized circuit for eddy current effects in transformer windings," *IEEE Trans. Power Del.*, vol. 28, no. 2, pp. 1063–1072, Apr. 2013.

[25] D. J. Wilcox, W. G. Hurley, and M. Conlon, "Calculation of self and mutual impedances between sections of transformer windings," *Proc. Inst. Elect. Eng.*, vol. 136, no. 5, pp. 308–314, Sep. 1989.

[26] W. G. Hurley and D. J. Wilcox, "Calculation of leakage inductance in transformer winding," *IEEE Trans. Power Electron.*, vol. 9, no. 1, pp. 121–126, Jan. 1994.

[27] J. A. Ferreira, "Improved analytical modeling of conductive losses in magnetic components," *IEEE Trans. Power Electron.*, vol. 9, no. 1, pp. 127–131, Jan. 1994.

[28] V. A. Niemela, G. R. Skutt, A. M. Urling, Y. Chang, T. G. Wilson, H. A. Owen, and R. C. Wong, "Calculating the short-circuit impedances of a multiwinding transformer from its geometry," in *Proc. IEEE Power Electron. Specialists Conf.*, 1989, pp. 607–617.

[29] R. W. Erickson and D. Maksimovic, "A multi-winding magnetics model having directly measurable parameters," in *Proc. IEEE Power Electron. Specialists. Conf.*, 1998, pp. 1472–1478.

[30] A. Morched, L. Marti, and J. Ottevangers, "A high frequency transformer model for the EMTP," *IEEE Trans. Power Del.*, vol. 8, no. 3, pp. 1615–1626, Jul. 1993.

[31] V. Brandwajn, H. W. Dommel, and I. I. Dommel, "Matrix representation of three-phase N-winding transformers for steady-state and transient studies," *IEEE Trans. Power App. Syst.*, vol. PAS-101, no. 6, pp. 1369–1378, Jun. 1982.

[32] C. Chimklai and J. R. Marti, "Simplified three-phase transformer model for electromagnetic transient studies," *IEEE Trans. Power Del.*, vol. 10, no. 3, pp. 1316–1325, Jul. 1995.

[33] A. Schellmanns, K. Berrouche, and J. Keradec, "Multiwinding transformer: A successive refinement method to characterize a general equivalent circuit," *IEEE Trans. Instrum. Meas.*, vol. 47, no. 5, pp. 1316–1321, Oct. 1998.

[34] J. M. Lopera, M. J. Prieto, A. M. Parnia, and F. Nuno, "A multiwinding modeling method for high frequency transformer and inductors," *IEEE Trans. Power Electron.*, vol. 18, no. 3, pp. 896–906, May 2003.

[35] M. Perry, *Low Frequency Electromagnetic Design*. New York, USA: Marcel Dekker, 1985.

[36] E. J. Tarasiewicz, A. S. Morched, A. Narang, and E. P. Dick, "Frequency dependent eddy current models for nonlinear iron cores," *IEEE Trans. Power Syst.*, vol. 8, no. 2, pp. 588–597, May 1993.

[37] P. Holmberg, A. Bergqvist, and G. Engdahl, "Modelling eddy currents and hysteresis in a transformer laminate," *IEEE Trans. Magn.*, vol. 33, no. 2, pp. 1306–1309, Mar. 1997.

[38] J. H. Krah, "Optimum discretization of physical cauer circuit," *IEEE Trans. Magn.*, vol. 41, no. 5, pp. 1444–1447, May 2005.

[39] F. de León, "Discussion of "Transformer modeling for low and mid-frequency transients—A review," *IEEE Trans. Power Del.*, vol. 23, no. 2, pp. 1625–1632, Apr. 2008.

[40] M. K. Kazimierczuk, *High-Frequency Magnetic Components*. Hoboken, NJ, USA: Wiley, 2009.

[41] R. P. Wojda and M. K. Kazimierczuk, "Winding resistance of litz-wire and multi-strand inductors," *IET Power Electron.*, vol. 5, no. 2, pp. 257–268, Feb. 2012.

[42] P. L. Dowell, "Effects of eddy currents in transformer windings," *Proc. Inst. Elect. Eng.*, vol. 113, pp. 1387–1394, Aug. 1966.

[43] D. Murthy-Bellur and M. K. Kazimierczuk, "Winding losses caused by harmonics in high-frequency flyback transformers for pulse-width modulated DC-DC converters in discontinuous conduction mode," *IET Power Electron.*, vol. 3, no. 5, pp. 804–817, Sep. 2010.

[44] D. Murthy-Bellur, N. Kondrath, and M. K. Kazimierczuk, "Transformer winding loss caused by skin and proximity effects including harmonics in pulse-width modulated DC-DC flyback converters for the continuous conduction mode," *IET Power Electron.*, vol. 4, no. 4, pp. 363–373, Apr. 2011.

[45] D. A. Nagarajan, D. Murthy-Bellur, and M. K. Kazimierczuk, "Harmonic winding losses in the transformer of a forward pulse width modulated DC-DC converter for continuous conduction mode," *IET Power Electron.*, vol. 5, no. 2, pp. 221–236, Feb. 2012.

[46] A. Rezaei-Zare, "Enhanced transformer model for low- and mid-frequency transients—Part I: Model development," *IEEE Trans. Power Del.*, vol. 30, no. 1, pp. 307–315, Feb. 2015.

[47] A. Rezaei-Zare, "Enhanced transformer model for low and mid-frequency transients—Part II: Validation and simulation results," *IEEE Trans. Power Del.*, vol. 30, no. 1, pp. 316–325, Feb. 2015.

[48] S. E. Zirka, Y. I. Moroz, and C. M. Arturi, "Accounting for the influence of the tank walls in the zero-sequence topological model of a three-phase, three-limb transformer," *IEEE Trans. Power Del.*, vol. 29, no. 5, pp. 2172–2179, Oct. 2014.

**Saeed Jazebi** (M'13), photograph and biography not available at the time of publication.

**Francisco de León** (F'15), photograph and biography not available at the time of publication.